

# Introducing the Fission-Fusion Reaction Process: Using a Laser-Accelerated Th Beam to produce Neutron-Rich Nuclei towards the $N = 126$ Waiting Point of the $r$ Process

D. Habs<sup>1,2</sup>, P.G. Thirolf<sup>1</sup>, M. Gross<sup>1</sup>, K. Allinger<sup>1</sup>, J. Bin<sup>1</sup>, A. Henig<sup>1</sup>, D. Kiefer<sup>1</sup>, W. Ma<sup>2</sup>, J. Schreiber<sup>2</sup>

<sup>1</sup> Fakultät für Physik, Ludwig-Maximilians Universität München, D-85748 Garching, Germany

<sup>2</sup> Max-Planck-Institut für Quantenoptik, D-85748 Garching, Germany

Received: date / Revised version: date

**Abstract** We propose to produce neutron-rich nuclei in the range of the astrophysical  $r$  process (the rapid neutron-capture process) around the waiting point  $N = 126$  [1,2,3] by fissioning a dense laser-accelerated thorium ion bunch in a thorium target (covered by a polyethylene layer, CH<sub>2</sub>), where the light fission fragments of the beam fuse with the light fission fragments of the target. Via laser Radiation Pressure Acceleration (RPA) [4,5] using a high-intensity, short pulse laser, very efficiently bunches of solid state density of <sup>232</sup>Th can be generated from a first Th production target (ca. 3.6 μm thick), placed on a CH<sub>2</sub> backing (ca. 24 μm). Laser accelerated Th ions with about 7 MeV/u will pass through a thin polyethylene layer placed in front of a thicker second Th foil closely behind the first target and desintegrate into light and heavy fission fragments. In addition light ions (p,C) from the CH<sub>2</sub> backing of the first Th target will be accelerated as well, inducing the fission process of <sup>232</sup>Th also in the second Th target. The laser-accelerated ion bunches with solid state density, which are about 10<sup>15</sup> times more dense than classically accelerated ion bunches, allow for a high probability that generated fission products can fuse again when the fragments from the thorium beam strike the second Th reaction target. In contrast to classical radioactive beam facilities, where intense but low-density radioactive beams of one ion species are merged with stable targets, the novel fission-fusion process draws on the fusion between neutron-rich, short-lived, light fission fragments both from beam and target. Moreover, the high ion beam density may lead to a strong collective modification of the stopping power in the target by 'snowplough-like' removal of target electrons, leading to significant range enhancement, thus allowing to use rather thick targets.

Using a high-intensity laser with 300 J and 15 fs pulse length (20 PW), as e.g. envisaged for the ELI-Nuclear Physics project in Bucharest (ELI-NP) [6], order-of-ma-

gnitude estimates promise a fusion yield of about 10<sup>4</sup> ions per laser pulse in the mass range of  $A = 180 - 190$ , thus enabling to approach the  $r$ -process waiting point at  $N=126$ . First studies on ion acceleration, collective modifications of the stopping behaviour and the production of neutron-rich nuclei can also be performed at the upcoming new laser facility CALA (Center for Advanced Laser Applications) in Garching.

## 1 Introduction

Elements like platinum and gold or thorium and uranium are produced via the rapid neutron capture process ( $r$  process) at astrophysical sites like merging neutron star binaries or (core collapse) supernova type II explosions with outbursts of very high neutron density in the range of  $10^{21} - 10^{30}/cm^3$ . We aim at improving our understanding of these nuclear processes by measuring the properties of heavy nuclei on (or near) the  $r$ -process path. According to a recent report by the US National Research Council of the National Academy of Science, the origin of the heaviest elements remains one of the 11 greatest unanswered questions of modern physics [7]. While the lower path of the  $r$  process for the production of heavy elements is well explored, the nuclei around the  $N = 126$  waiting point critically determine this element production mechanism, and at present basically nothing is known about these nuclei.

Special ingredients of this proposal are: i) The very efficient Radiation Pressure Acceleration (RPA) mechanism for laser-based ion acceleration, producing pancake-like beam bunches of solid state density. ii) The strongly reduced stopping power of these dense bunches in a second thick Th target, where the decomposition into fission fragments and the fusion of these fragments takes place. After the laser flash we want to extract rather

Send offprint requests to:

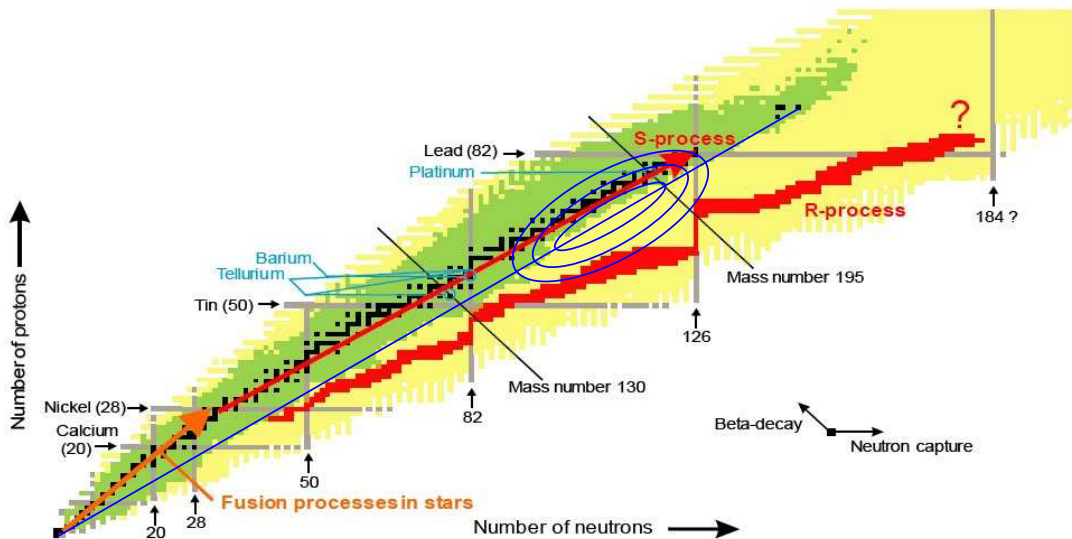


**Fig. 1** Chart of the nuclides indicating various pathways for astrophysical nucleosynthesis: thermonuclear fusion reactions in stars (orange vector), *s*-process path (red vector) and the *r* process generating heavy nuclei in the Universe (red pathway). The nuclei marked in black indicate stable nuclei. For the green nuclei some nuclear properties are known, while the yellow, yet unexplored regions extend to the neutron and proton drip lines. The blue line connects nuclei with the same neutron/proton ratio as for (almost) stable actinide nuclei. On this line the maximum yield of nuclei produced via fission-fusion (without neutron evaporation) will be located. The elliptical contour lines correspond to the expected maximum fission-fusion cross sections decreased to 50%, 10% and 0.1%, respectively, for primary  $^{232}\text{Th}$  beams.

long-lived isotopes ( $> 100$  ms) in flight, separate them e.g. in a (gas-filled) recoil separator and study them via decay spectroscopy or lifetime and nuclear mass measurements.

In the following we outline the relevance of the project for nuclear astrophysics, describe the new laser acceleration scheme and in particular the new fission-fusion reaction method. Finally the planned ELI-Nuclear Physics facility will be briefly introduced, where the production of these nuclei and the experiments to measure their properties will be realized.

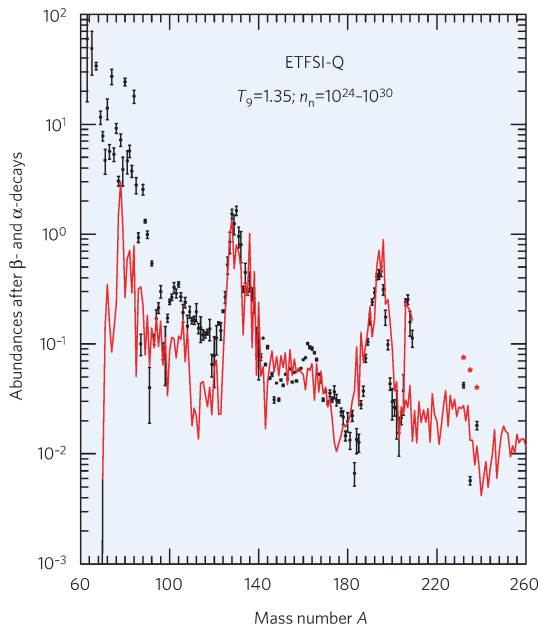
## 2 The Relevance of the $N=126$ Waiting Point for Nuclear Astrophysics

Fig. 1 shows the nuclidic chart marked with different nucleosynthesis pathways for the production of heavy elements in the Universe: the thermonuclear fusion processes in stars producing elements up to iron (orange arrow), the slow neutron capture process (*s* process) along the valley of stability leading to about half of the heavier nuclei (red arrow) and the rapid neutron capture process (*r* process) proceeding along pathways with neutron separation energies  $S_n$  in the range of 2–3 MeV. In this scenario rather neutron rich nuclei are populated in an intense neutron flux [8]. The *r* process path exhibits characteristic vertical regions for constant magic neutron numbers of 50, 82 and 128, where the *r* process is slowed down due to low neutron capture cross sections when going beyond the magic neutron numbers. These deci-

sive bottlenecks of the *r* process flow are called waiting points [9].

The astrophysical site of the *r*-process nucleosynthesis is still under debate: it may be cataclysmic core collapse supernovae (II) explosions with neutrino winds [2, 3, 10, 11] or mergers of neutron-star binaries [12, 13, 14]. The *r*-process element abundances from galactic halo stars tell us that the *r*-process site for lighter and heavier neutron capture processes may occur under different astrophysical conditions [9]. For the heavier elements beyond barium the isotopic abundances are always very similar (called universality) and the process seems to be very robust. Perhaps also the recycling of fission fragments from the end of the *r* process strengthens this stability. Presently it seems more likely that a merger of neutron star binaries is the source for the heavier *r*-process branch, while core collapsing supernova explosions contribute to the lighter elements below barium. The modern nuclear equations of state, neutrino interactions and recent supernova explosion simulations [3] lead to detailed discussions of the waiting point  $N=126$ . Here measured nuclear properties along the  $N=126$  waiting point may help to clarify the sites of the *r* process.

Fig. 2 shows the measured solar elemental abundances of the *r*-process nuclei together with a calculation, where masses from the Extended Thomas-Fermi plus Strutinski Integral (ETFSI) mass model [15] have been used together with several neutron flux components, characterized by a temperature  $T_9$ , neutron densities  $n_n$  and expansion time scales. A quenching of shell effects [17] was assumed in the nuclear mass calculations to achieve a



**Fig. 2** Observed elemental solar abundances in the  $r$  process mass range (black symbols with error bars) in comparison with calculated abundances (red line and symbols). The theoretical predictions show the elemental abundances for stable isotopes after  $\alpha$  and  $\beta$  decay as obtained in the ETFSI-Q mass model [1, 15] for a wide range of neutron densities  $n_n$  (in  $1/cm^3$ ) and temperatures  $T_9$  (in units of  $10^9 K$ ) and including shell quenching effects. Included with permission from [16].

better agreement between observed and calculated abundances. We note the pronounced third peak in the abundance distribution around  $A = 180 - 200$ , corresponding to the group of elements around gold, platinum and osmium, where until now no experimental nuclear properties have been measured for  $r$ -process nuclei. The key bottleneck nuclei of the  $N=126$  waiting point around  $Z \approx 70$  are about 15 neutrons away from presently known nuclei (see Fig. 1), with a typical drop of the production cross section for classical radioactive beam production schemes of about a factor of 10-20 for each additional neutron towards more neutron-rich isotopes. Thus presently nothing is known about these nuclei and even next-generation large-scale 'conventional' radioactive beam facilities like FAIR [18], SPIRAL II [19] or FRIB [20] will not be able to grant experimental access to the most important isotopes on the  $r$  process path. The third peak in the abundance curve of  $r$ -process nuclei is due to the  $N = 126$  waiting point as visible in Fig. 1. These nuclei are expected to have rather long half-lives of a few 100 ms. This waiting point represents the bottleneck for the nucleosynthesis of heavy elements up to the actinides. From the view point of astrophysics it is the last region, where the  $r$ -process path gets close to the valley of stability and thus can be studied with the new isotopic production scheme discussed below. While the waiting point nuclei at  $N = 50$  and  $N = 82$  have been studied rather extensively [21, 22, 23, 24], nothing is known experimen-

tally about the nuclear properties of waiting point nuclei at the  $N = 126$  magic number. Nuclear properties to be studied here are nuclear masses, lifetimes,  $\beta$  delayed neutron emission probabilities  $P_{\nu,n}$  and the underlying nuclear structure.

For the overall description of the  $r$  process the nuclear masses are typically taken from mass models like the macroscopic-microscopic Finite Range Droplet Model (FRDM). Alternatively models more closely related to first principles like Hartree-Fock-Bogoliubov calculations are used [9, 2]. Typically somewhat less shell quenching is assumed for the heavier  $N=126$  region compared to the  $N=82$  region of the  $r$  process.

Fig. 3 displays the difference between nuclear masses for the isotopic chain  $Z = 55$  (Cs) as calculated by various mass models and measured masses (data taken from AME95 [25]). The plot demonstrates the good agreement between measured and predicted masses in the mass range where experimental data are available, while drastic deviations occur outside these regions especially for the  $r$ -process region [24]. For the Cs isotopes with  $Z=55$  as shown in Fig. 3 the mass measurements reach close to the  $r$ -process path. However, for the heavier elements relevant for the  $r$  process waiting point  $N=126$  around  $Z \approx 70$ , the known isotopes are about 15 neutrons away from the magic neutron number  $N = 126$  and Fig. 3 impressively illustrates the extremely large uncertainties presently expected for any theoretical prediction of nuclear masses,  $Q$  values or  $\beta$  half-lives which may partly be attributed to effects of nuclear deformation. This clearly points to the importance of direct measurements in this mass region, especially targeting nuclear masses.

Moreover, presently there exist difficulties to describe consistently the third abundance peak of the  $r$  process, the  $^{232}\text{Th}$  and  $^{238}\text{U}$  cosmochronometers and the potential 'fission cycle' beyond  $A > 260$  [26].

From the viewpoint of nuclear structure theory semi-magic, heavy nuclei not too far away from stability are spherical and thus can be treated in general more successfully than heavy deformed nuclei. Shell model calculations with open proton- and neutron shells require extremely large dimensions of the configuration space. With realistic density functional theories some extremely time consuming deformed RPA calculations with Skyrme or Gogny forces have been performed [27], but still spherical nuclei can be controlled much better. Also the subsystem of neutrons or protons allows to study systems with large isospin. These density functional calculations have to be fitted to experimental data of heavy nuclei, in order to enable reliable predictions for other nuclei [27]. If we improve our experimental understanding of this final bottleneck to the actinides at  $N=126$ , many new visions open up: (i) for many mass formulas (e.g. [28]) there is a branch of the  $r$  process leading to extremely long-lived superheavy elements beyond  $Z=110$  with lifetimes of about  $10^9$  years. If these predictions could be

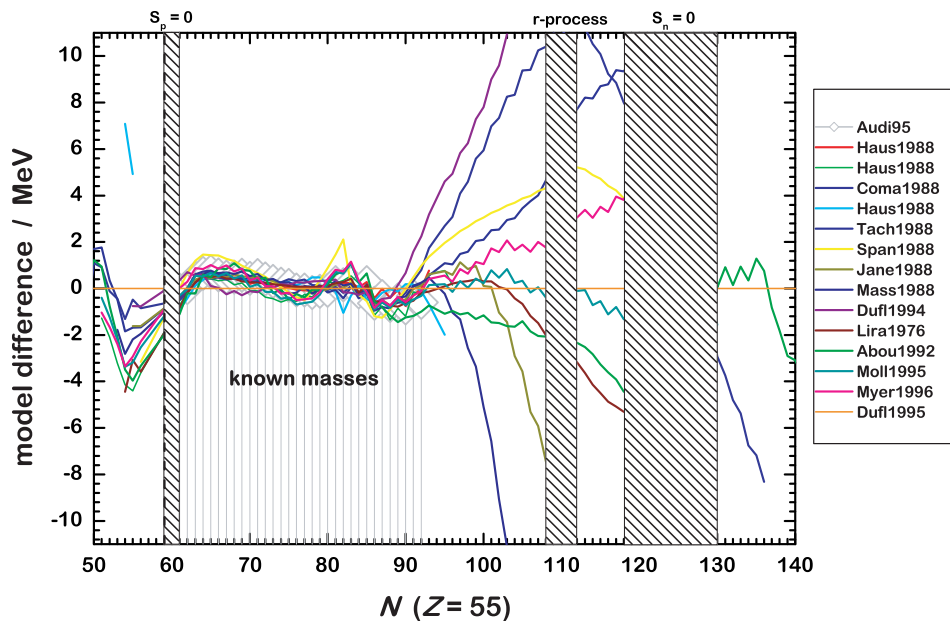


**Fig. 3** Differences between nuclear mass predictions from various theoretical mass models for Cs isotopes ( $Z=55$ ) compared to measured masses taken from AME95 [25] as a function of the mass number  $A$ . The figure is taken with permission from Ref. [24].

made more accurate, a search for these superheavy elements in nature would become more promising. (ii) at present the prediction for the formation of uranium and thorium elements in the  $r$  process is rather difficult, because there are no nearby magic numbers and because those nuclei are formed during a fast passage of the nuclidic area between shells. Such predictions could be improved, if the bottleneck of actinide formation would be more reliably known. (iii) also the question could be clarified if fission fragments are recycled in many  $r$ -process loops or if only a small fraction is reprocessed. This description of our present understanding of the  $r$  process underlines the importance of the present project for nuclear physics and particularly for astrophysics.

### 3 The Fission-Fusion Reaction Process

In the following section the various ingredients enabling the new fission-fusion reaction scenario are outlined. First the 'Radiation Pressure Acceleration' method of laser ion acceleration is described, which allows to generate ultra-dense ion beams. Consequently collective effects are expected for the interaction of these ion beams with solid targets, leading to a significant reduction of the conventional electronic stopping power. Finally the fission-fusion reaction process based on these ultra-dense laser-accelerated ion beams is described and an order-of-magnitude estimate for the achievable fusion yield will be presented.

#### 3.1 Laser Ion Acceleration

Laser-accelerated energetic ion beams have been produced during the last few years from  $\mu\text{m}$  thick metallic foils when irradiated by ultra-intense, short laser pulses [29,30,31]. In these experiments the high energy electrons produced at the front of the target penetrated the target, which is opaque to the laser. At the rear side the electrons generate an electrostatic field, which ionizes and accelerates ions from the rear side. This acceleration mechanism was called 'Target Normal Sheath Acceleration (TNSA)'. It was explored in many experiments at various high-intensity laser laboratories [32,33,34,35]. A recent review [36] shows that the ion energy scales proportional to the square root of the laser intensity. Typical conversion efficiencies from laser energy to ion energy amount to less than 1%.

In the proposal of a new nuclear reaction scenario introduced in this work we envisage to exploit instead the new Radiation Pressure Acceleration (RPA) mechanism for ion acceleration. It was first proposed theoretically [37,38,39]. The experimental verification of these predictions was achieved only recently in experiments led by the Munich group [4,5,40]. The RPA laser ion acceleration mechanism provides a much larger efficiency for the conversion from laser energy to ion energy and allows for a generation of much larger ion energies in comparison to TNSA. Moreover, for circularly polarized laser light RPA holds promise of quasi-monoenergetic ion beams. Due to the circular polarization electron heating is strongly suppressed. The electrons are compressed to a dense electron sheet in front of the laser pulse, which then via the rectified dipole field accelerates the ions.

This mechanism requires much thinner targets and ultra-high contrast laser pulses to avoid the pre-heating and expansion of the target before the interaction with the main laser pulse.

The RPA mechanism allows to produce ion bunches with solid state density ( $10^{24}/\text{cm}^3$ ), which thus are  $\approx 10^{15}$  times more dense than ion bunches from classical accelerators. Correspondingly the areal densities of these bunches are  $\approx 10^8$  times larger. It is important to note that these ion bunches are accelerated as neutral ensembles together with the accompanying electrons and thus do not Coulomb explode.

While in previous experiments a conversion efficiency of laser energy to ion energy of 12% [40] for carbon beams could be achieved when using a rather moderately intense laser of 30 TW and 0.7 Joule, we expect a significantly larger conversion efficiency of about 50% for e.g. a 20 PW laser. In the scenario discussed in this work we aim at accelerating heavier Th ions with  $A=232$  and focus the laser to a spot size of  $3 \mu\text{m}$  diameter.

The optimum bunch diameter and the bunch length are important parameters, since the bunch diameter controls which fraction of the opening cone of the beam-like fission fragments may leave the interaction volume. The length of the bunch controls the number of target-like fission products in the interaction volume. With a larger laser energy both parameters could be increased, leading to a nonlinear increase of the yield of neutron-rich fusion products.

For the high intensity 20 PW APOLLON laser with 300 J, which is presently developed at the ENSTA/Ecole Polytechnique in Palaiseau near Paris within the ILE project [41] and which will form the backbone of the ELI-Nuclear Physics project currently starting the design phase in Bucharest, we expect to accelerate  $10^{12}$  Th ions with an energy of about 7 MeV/u in a pancake-shaped bunch with  $3 \mu\text{m}$  diameter and  $3.6 \mu\text{m}$  length.

### 3.2 Stopping Power for Dense Ion Bunches in a Solid Target

In nuclear physics the Bethe-Bloch formula [42] is used to calculate the atomic stopping of energetic individual ions

$$-dE/dx = 4\pi n_e \frac{Z_{eff}^2 e^4}{m_e v^2} [\ln(2m_e v^2 / I(1 - (v/c)^2)) - (v/c)^2] \quad (1)$$

where  $I$  denotes the ionization potential,  $n_e$  the density of the electrons,  $m_e$  the mass of the electron, while  $v$  is the ion velocity and  $Z_{eff}$  is the effective charge of the ions.

For laser accelerated ions the ion bunch densities reach solid state densities, which are about 15 orders of magnitude larger compared to beams from classical accelerators. In such a scenario collective effects become

important. The Bethe-Bloch equation can be decomposed according to Ref. [43] into a first part describing binary collisions and a second term describing long range collective contributions according to

$$-dE/dx = 4\pi n_e \frac{Z_{eff}^2 e^4}{m_e v^2} [\ln(m_e v^2 / e^2 k_D) + \ln(k_D v / \omega_p)] \quad (2)$$

Here  $k_D$  is the Debye wave number and  $\omega_p$  is the plasma frequency of the electrons. In Ref. [44] the mechanism of collective deceleration of a dense particle bunch in a thin plasma is discussed, where the particle bunch fits into part of one plasma oscillation and is decelerated  $10^5 - 10^6$  times stronger than predicted by the classical Bethe-Bloch equation [42] due to a strong collective wakefield. Now we discuss the opposite effect with a strongly reduced atomic stopping power that occurs when sending the energetic, solid state density ion bunch into a solid carbon or thorium target. For this target the plasma wavelength ( $\lambda_p \approx 1 \text{ nm}$ ) is much smaller than the ion bunch length ( $\approx 3.6 \mu\text{m}$ ) and collective acceleration and deceleration effects cancel. Only the binary collisions remain and contribute to the stopping power. Hence, we may consider the dense ion bunch as consisting of about  $1.1 \cdot 10^4$  atomic layers with a distance between the Th ions of about  $3.2 \text{ \AA}$  as obtained from the bulk density of metallic thorium ( $11.7 \text{ g/cm}^3$ ). In this case the first layers of the ion bunch will attract the electrons from the target and like a snow plough will take up the decelerating electron momenta. Hence the predominant part of the ion bunch is screened from electrons and we expect a drastic reduction of the stopping power. The electron density  $n_e$  will be strongly reduced in the channel defined by the laser-accelerated ions, because many electrons are expelled by the ion bunch and the laser pulse. This effect requires detailed experimental investigations planned for the near future, aiming at verifying the perspective to use a significantly thicker reaction target. The classical ion range for e.g. 7 MeV/u thorium ions in carbon is  $15 \text{ mg/cm}^2$ , corresponding to a range of  $66 \mu\text{m}$ , while this range amounts to only  $40 \mu\text{m}$  in a thorium target. However, if we aim at limiting the usable effective range to a thorium target thickness where the remaining projectile energy is still sufficient to induce fission, using the accelerated thorium ions directly to induce fission in the Th target would result in a usable target range of less than  $10 \mu\text{m}$  without invoking collective effects. However, the use of proton induced fission leads to a usable target thickness of about  $50 \mu\text{m}$ .

The expected reduced atomic stopping power will be supported by the strong laser heating of the electrons. A reduction of the atomic stopping is essential to avoid a strong slowing down of the ions below the Coulomb barrier energies, where nuclear reactions are no longer possible. However, even without this reduced stopping power the basic properties of the novel reaction mechanism could still be studied, however with significantly

reduced yields.

Taking collective effects into account by assuming a range enhancement by a factor of 100, we expect a usable thickness of several mm for a thorium target.

An optimized ion acceleration scheme will depend on measured stopping powers of the dense bunches in targets of different materials and thicknesses, including the ion beam energy as a further parameter to be optimized in preparatory studies.

### 3.3 The Fission-Fusion Process

The basic concept of the fission-fusion reaction scenario draws on the ultra high density of laser-accelerated ion bunches. Choosing fissile isotopes as target material for a first target foil accelerated by an intense laser pulse will enable the interaction of a dense beam of fission fragments with a second target foil also consisting of fissile isotopes. So finally in a second step of the reaction process fusion between (neutron-rich) beam-like and target-like fission products will become possible, generating extremely neutron-rich ion species.

For our discussion we choose  $^{232}\text{Th}$  (the only component of chemically pure Th) as fissile target material, primarily because of its long half-life of  $1.4 \cdot 10^{10}$  years, which avoids extensive radioprotection precautions during handling and operation. Moreover, metallic thorium targets are rather stable in a typical laser vacuum of  $10^{-6}$  mbar, whereas e.g. metallic  $^{238}\text{U}$  targets would quickly oxidize.

Nevertheless in a later stage it may become advantageous to use also heavier actinide species in order to allow for the production of even more exotic fusion products.

In general the fission process of the two heavy Th nuclei from beam and target will be preceded by the deep inelastic transfer of neutrons between the inducing and the fissioning nuclei. Here the magic neutron number in the superdeformed fissile nucleus with  $N=146$  [45,46] may drive the process towards more neutron-rich fissioning nuclei, because the second potential minimum acts like a doorway state towards fission. Since in the subsequent fission process the heavy fission fragments keep their  $A$  and  $N$  values [47], these additional neutrons will show up in the light fission fragments and assist to reach more neutron-rich nuclei. This process will be of particular importance in the reaction scenario discussed in Sect. 3.3.2 for the case of collectively reduced stopping in the reaction target.

Fig. 4 shows a sketch of the proposed fission-fusion reaction scenario for two different situations, a) for the case of normal electronic stopping as described by the Bethe-Bloch equation and b) for the case of reduced stopping due to collective effects in the target induced by the ultra-dense ion beam discussed earlier. The latter scenario will be discussed later.

A short-pulse, high-intensity laser pulse is focused onto a first target foil, the production target. We discuss in the following an experimental scenario for the 300 J, 15 fs APOLLON laser, which is envisaged for the ELI-NP project in Bucharest. The corresponding 20 PW of laser power will be focused with about  $10^{23}\text{W}/\text{cm}^2$  to a focal spot with a diameter of about  $3\ \mu\text{m}$  on the first  $^{232}\text{Th}$  target ('production target'), which is deposited on a  $\text{CH}_2$  backing foil with a thickness of about  $24\ \mu\text{m}$ . The optimum thickness of this first thorium target is determined by the available laser energy and the envisaged energy of the laser-accelerated thorium ion beam. Based on a conversion efficiency of about 50% from laser energy to accelerated ion energy, about  $10^{12}$  thorium ions can be accelerated with solid state density via the above described RPA acceleration mechanism to energies of about 7 MeV/u. Here the resulting energy of the laser accelerated ions can be adjusted via the choice of the laser focus conditions, since for the RPA mechanism the ion energy scales linearly with the laser intensity and hence with the square of the normalized laser amplitude  $a$ .

Within the chosen laser focal spot of  $3\ \mu\text{m}$  diameter one atomic layer (with a distance between thorium atoms of about  $3.2\ \text{\AA}$  as derived from the bulk density) corresponds to  $9 \cdot 10^7$  thorium ions. Therefore the accelerated  $10^{12}$  ions with solid state density correspond to  $1.1 \cdot 10^4$  atomic layers, resulting in an optimized thickness of the thorium production target of about  $3.6\ \mu\text{m}$ .

At the same time also the light ions from the  $\text{CH}_2$  backing (p,C) will be accelerated to the same energy per nucleon. In this case about  $2 \cdot 10^{13}$  protons and  $10^{13}$  carbon ions can be accelerated, which subsequently will be used to induce fission in a second, much thicker Th reaction target placed behind the first production target in a much more efficient way compared to a scenario, where directly the accelerated thorium ions would be used to induce fission in the reaction target.

The required distance between production and reaction target assembly is determined by the requirement that the laser pulse that penetrates the production target should not affect or even destroy the reaction target. The quantity to be considered here is the Rayleigh length of the focused laser light, which indicates the distance from the laser focus where the intensity drops by a factor of two. In order to achieve a drop of intensity from  $10^{23}\text{W}/\text{cm}^2$  by about a factor of 1000, which leads to an intensity that can be tolerated by the reaction target, at least 10 Rayleigh lengths have to be allowed between production and reaction target. The Rayleigh length  $z_0$  is given by  $z_0 = \pi w_0^2 / \lambda$  with  $w_0$  given by the laser spot diameter of  $3\ \mu\text{m}$  in our case and  $\lambda$  being the laser wavelength of  $1\ \mu\text{m}$ . Thus the Rayleigh length in our case amounts to about  $30\ \mu\text{m}$  and the reaction target should be placed at least  $0.3\ \text{mm}$  behind the production target. Thus we propose to place the reaction target  $0.5\ \text{mm}$  behind the production target, as indicated in Fig. 4.

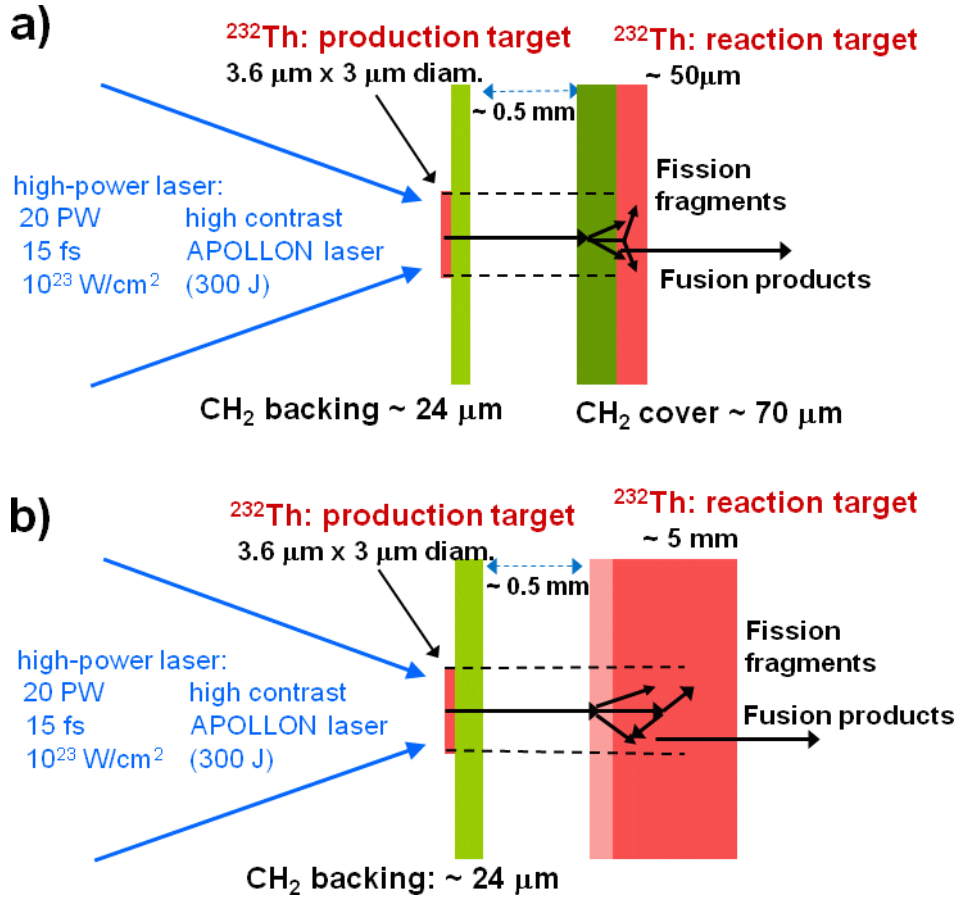


**Fig. 4** Sketch of the target arrangement envisaged for the fission-fusion reaction process based on laser ion acceleration. Part a) illustrates the situation in case no collective effects on the electronic stopping are taken into account. In this case the thickness of the carbon layer as well as the second thorium reaction target have to be limited to about 30-50  $\mu\text{m}$  in order to enable fission of beam and target nuclei. This will allow for fusion between their light fragment as well as enable the fusion products to leave the second thorium reaction target. Part b) depicts an alternative scenario, where we consider also collective effects in the reaction target induced by the ultra-dense ion bunches. Here the first part of the thorium reaction target is used to decelerate the fission fragments from about 7 MeV/u to about 3 MeV/u, suitable for efficient fusion of neutron rich species. Due to the reduced electronic stopping a larger target thickness and thus increased fission and fusion yields can be expected. Further details are discussed in the text.

### 3.3.1 Induced fission with normal electronic stopping

In a scenario, where the earlier discussed collective effects in the target are not taken into account (marked with 'a') in Fig. 4), the second thorium reaction target would have a thickness of about 50  $\mu\text{m}$ .

Using a distance of 2.8  $\text{\AA}$  between atoms in solid layers of  $\text{CH}_2$ , the accelerated light ion bunch ( $10^{13}$  ions) corresponds to  $8.7 \cdot 10^4$  atomic layers in case of a 24  $\mu\text{m}$  thick  $\text{CH}_2$  backing. In order to allow for an optimized fission of the accelerated Th beam, the second, thicker Th reaction target which is positioned behind the production target is covered by about 70  $\mu\text{m}$  of polyethylene. This layer serves a twofold purpose: primarily it is used to induce fission of the impinging Th ion beam, generating the beam-like fission fragments. Here polyethylene is advantageous compared to a pure carbon layer because of the increased number of atoms able to induce fission on the impinging Th ions. In addition the thickness of this second  $\text{CH}_2$  layer has been chosen such that the pro-

duced fission fragments will be decelerated to a kinetic energy which is suitable for optimized fusion with the target-like fission fragments generated by the light accelerated ions in the second Th target, minimizing the amount of evaporated neutrons. After each laser shot a new double-target has to be rotated into position.

In order to estimate the fission cross sections both of beam and target nuclei, we apply geometrical considerations based on the involved nuclear radii, which can be expressed for mass number  $A$  in the usual way as

$$R = 1.2 * (A)^{1/3} fm \quad (3)$$

Neglecting the influence of surface diffuseness effects, the resulting fission cross section of the  $^{232}\text{Th}$  beam in the  $\text{CH}_2$  layer of the reaction target assembly amounts to  $\sigma_{\text{fis}} = \pi(R_1 + R_2)^2 = 350 \text{ fm}^2 = 3.5 \cdot 10^{-28} \text{ m}^2$  (3.5 b). Correspondingly the proton-induced fission in

the Th reaction target occurs with a cross section of about  $230 \text{ fm}^2 = 2.3 \cdot 10^{-28} \text{ m}^2$  (2.3 b). If we use the atomic distance of  $3.2 \text{ \AA}$  for thorium, we conclude a fission probability of about  $3.8 \cdot 10^{-9}$  per atomic layer.

In order to estimate the required thickness of the  $\text{CH}_2$  layer in front of the Th reaction target, we have to take into account the range of the  $7 \text{ MeV/u } ^{232}\text{Th}$  ions, which is about  $120 \text{ }\mu\text{m}$ . However, already after  $70 \text{ }\mu\text{m}$  the kinetic energy of the Th ions has dropped to  $3 \text{ MeV/u}$ , which is about the energy required for the resulting fission fragments during the subsequent fusion step. Therefore we estimate a thickness of the polyethylene layer of about  $70 \text{ }\mu\text{m}$ , which corresponds to about  $2.5 \cdot 10^5$  atomic layers. Together with the above estimated fission probability per atomic layer and taking into account that from  $\text{CH}_2$  three atoms will contribute to the fission process of the impinging Th beam, this results in a fission probability for the Th ion beam of about  $2.9 \cdot 10^{-3}$  in the  $70 \text{ }\mu\text{m}$   $\text{CH}_2$  layer, thus generating about  $2.9 \cdot 10^9$  beam-like fission fragments per laser pulse.

The 99.7% of Th beam ions surviving the  $\text{CH}_2$  layer will enter the Th reaction target with about  $2.4 \text{ MeV/u}$ , corresponding to a range of  $21 \text{ }\mu\text{m}$ . In the first Th target layers a fraction of them will undergo fission before being slowed down too much, however, the resulting fragment energies will not be suitable for the fusion step. A quantitative assessment of this component would require detailed simulations and will be finally addressed by experimental studies.

In general the fission process proceeds asymmetric [47]. The heavy fission fragment for  $^{232}\text{Th}$  is centred at  $A=139.5$  (approximately at  $Z=54.5$  and  $N=84$ ) close to the magic numbers  $Z=50$  and  $N=82$ . Accordingly, the light fission fragment mass is adjusted to the mass of the fixed heavy fission fragment, thus resulting for  $^{232}\text{Th}$  in  $A_L=91$  with  $Z_L \approx 37.5$ . During the fission process of  $^{232}\text{Th}$  for low excitation energies typically 1.6 neutrons are emitted. However, for the discussion presented here we neglect this loss of neutrons, because 4 or 5 neutrons may be transferred to the fissioning nucleus in the preceding transfer step (particularly efficient and thus important in case of the Th-induced fission discussed in the following section). The width (FWHM) of the light fission fragment peak is typically  $\Delta A_L = 14$  mass units, the 1/10 maximum width about 22 mass units [47].

So far we have considered the fission process of beam-like Th nuclei in the  $\text{CH}_2$  layer of the reaction target assembly. Similar arguments can be invoked for the proton (and carbon) induced generation of (target-like) fission products in the subsequent thicker thorium reaction target.

Reduced by the energy loss of the  $\sim 7 \text{ MeV}$  protons from the  $\text{CH}_2$  backing of the production target, proton induced fission from about  $6.5 \text{ MeV}$  protons will occur in the  $^{232}\text{Th}$  reaction target. Since we can consider the  $2 \cdot 10^{13}$  laser-accelerated protons (plus  $10^{13}$  carbon

ions) impinging on the second target per laser pulse as  $8.7 \cdot 10^4$  consecutive atomic layers, we conclude a corresponding fission probability in the second Th target of about  $\cdot 10^{-3}$ . A thickness of the thorium reaction target of about  $50 \text{ }\mu\text{m}$  could be exploited, where the kinetic proton energy would be above the Coulomb barrier to induce fission over the full target depth.

An essential effect to be taken into account is the widening of the fission fragment beam, because a kinetic energy of about  $1 \text{ MeV/u}$  is added to the fission fragments in arbitrary directions. However, the angular distribution of fission fragments from proton (or heavy ion) induced fission follows a  $1/\sin(\Theta)$  distribution [47] and thus fragments are predominantly emitted in beam direction. Consequently, a fraction of a few percent will stay within the cylinder volume defined by the small spot diameter defined by the laser focus on the first Th target.

Due to the additional kinetic energy of about  $1 \text{ MeV/u}$  of the fission fragments in the thick second target also the target-like fragment volume will expand. Here the very short bunch length of the fragment beam becomes important. The beam velocity is about 10% of the velocity of light and during the short fly-by time of the ions of only 1 fs the fission fragments of the target can only move a distance of  $1 \text{ }\mu\text{m}$ , which is still small compared to the beam diameter of  $3 \text{ }\mu\text{m}$ . Thus this enlargement of the target area is negligible.

In a second step of the fission-fusion scenario we consider the fusion between the light fission fragments of beam and target to a compound nucleus with a central value of  $A \approx 182$  and  $Z \approx 75$ .

Again we employ geometrical arguments for an order-of-magnitude estimate of the corresponding fusion cross section. For a typical light fission fragment with  $A = 90$  the nuclear radius can be estimated as  $5.4 \text{ fm}$ . Considering a thickness of  $50 \text{ }\mu\text{m}$  for the second Th reaction target that will be converted to fission fragments, equivalent to  $1.6 \cdot 10^5$  atomic layers, this results in a fusion probability of about  $1.8 \cdot 10^{-4}$ .

With this estimate for the fusion cross section we can finally derive an order-of-magnitude for the final yield of fusion products generated via the presented fission-fusion process of about  $5 \cdot 10^2$  fusion products per laser shot. This estimate does not yet take into account any collective effects in the target that might result in much higher fission rates and accordingly increased fusion yields as discussed in the following section.

Besides the fusion of two light fission fragments other reactions may happen. The fusion of a light fission fragment and a heavy fission fragment would lead back to the original Th nuclei, with large fission probabilities, thus we can neglect these fusion cross sections. The fusion of two heavy fission fragments would lead to nuclei with  $A \approx 278$ , again nuclei with very high fission probability. Hence we have also neglected these rare fusion

cross sections, although they may be of interest on their own. Thus we concentrate here only on the fusion of two light fission fragments. Besides studying nuclei close to the waiting point of the  $r$  process with the magic neutron number  $N=126$ , we may investigate also neutron-rich isotopes with the magic proton number  $Z=82$ , which are of large interest in nuclear structure studies.

Very neutron-rich nuclei still have comparably small production cross sections, because weakly bound neutrons ( $B_N \geq 3$  MeV) will be evaporated easily. The optimum range of beam energies for fusion reactions resulting in neutron-rich fusion products amounts to about 2.8 MeV/u according to PACE4 [49] calculations. So e.g. the fusion of two neutron-rich  $^{98}_{35}\text{Br}$  fission products with a kinetic energy of the beam-like fragment of 275 MeV leads with an excitation energy of about 60 MeV to a fusion cross section of 13 mb for  $^{189}_{70}\text{Yb}_{119}$ , which is already 8 neutrons away from the last presently known Yb isotope.

One should note that the well-known hindrance of fusion for nearly symmetric systems (break-down of fusion) only sets in for projectile and target masses heavier than 100 amu [50,51]. Thus for the fusion of light fission fragments we expect an unhindered fusion evaporation process.

In Fig. 1 the range of reachable fusion products from the fission-fusion process is indicated by the blue ellipses overlaid to the chart of nuclides. The proton to neutron ratio, which is approximately conserved during fission (indicated by the straight blue line connecting  $^1\text{H}$  with  $^{238}\text{U}$ ) determines the slope of the inner blue elliptical contour in Fig. 1. Their eccentricity reflects the region of nuclei reachable within a range of 50% of the maximum fusion cross section, based on the large fluctuations of proton and neutron numbers of the participating fission fragments. So far the dimensions of the contour lines drawn in Fig. 1 and Fig. 5 have been estimated from usual fission distributions. Since the mass distributions of both light fission fragments exhibit a certain width (FWHM), the width of the resulting distribution after fusion will be about a factor of  $\sqrt{2}$  larger. Those distributions will steepen when reaching further out to their tails. The other two elliptical contour lines correspond to the regions of fusion products expected to be reachable with 10% and  $10^{-3}$  of the maximum cross sections, respectively.

Fig. 5 displays a closer view into the region of nuclides around the  $N=126$  waiting point of the  $r$  process, where nuclei on the  $r$  process path are indicated by the green colour, with dark green highlighting the key bottleneck  $r$  process isotopes [52] at  $N=126$  between  $Z=66$  (Dy) and  $Z=70$  (Yb). One should note that e.g. for Yb the presently last known isotope is 15 neutrons away from the  $r$ -process path at  $N=126$ . The isotopes in light blue mark those nuclides, where recently  $\beta$  half-lives could be measured following projectile fragmentation and in-flight separation at GSI [53]. Again the elliptical contour

lines indicate the range of nuclei accessible with our new fission-fusion scenario on a level of 50%, 10% and  $10^{-3}$  of the maximum fusion cross section between two neutron-rich light fission fragments in the energy range of about 2.8 MeV/u, respectively.

*3.3.2 Fission-Fusion with collectively reduced electronic stopping* So far we estimated the expected fission and fusion yield without referring to any collective effects in the reaction targets that may reduce the electronic stopping as discussed earlier. Now we extend this discussion by considering the expected reduction of the electronic stopping in the reaction target. This scenario would allow to extend the Th target thicknesses to probably a few mm (situation 'b') in Fig. 4).

While so far no experimental data or quantitative assessment on the amount of collective range enhancement is available, we assume for this section a factor of 100 and discuss the consequences.

In contrast to the previously discussed scenario without collective effects we now propose to abandon the carbon layer in front of the Th reaction target and use only a homogeneous, thick Th target as indicated in Fig. 4b). In this case we use the first part of the target primarily as stopping medium for the incoming energetic Th ions in order to decelerate them from initially about 7 MeV/u to about 3 MeV/u, which is suitable for the subsequent fusion step with target-like fragments from proton-induced fission. Since such a deceleration could be reached in about 16  $\mu\text{m}$  without collective effects, we estimate here about 0.2 mm from our 5 mm thick Th reaction target acting as stopper while producing fission fragments too fast for efficient fusion of extremely neutron-rich isotopes. This part of the reaction target is marked by the shaded red colour in Fig. 4b). However, this part amounts to only 4% of the reaction target and thus does not lead to a significant loss of usable fission yield. On the other hand neutron transfer towards the deformed neutron shell closure at  $N=146$  preceding fission will add 4 neutrons to the light fission fragment and thus significantly help to enhance fusion of very neutron-rich isotopes. Compared to the situation of Fig. 4a) a thickness of the thorium target increased by a factor of 100 to about 5 mm due to the correspondingly reduced stopping would result in a full conversion of the Th beam into fission fragments (with  $\sim 96\%$  in an energy range usable for the fusion step). Thus  $10^{12}$  beam-like light fission fragments would become available for the fusion stage of the reaction process.

Consequently the proton-induced fission yield in the reaction target would also rise by the same factor of 100 to a target fission probability of 0.1. Here we use the assumption of a linear rise of the energy loss with target thickness, preserving a kinetic proton energy above the fission barrier to induce fission over the full target depth.

So we conclude that the expected collective stopping range enhancement will lead to a drastic increase

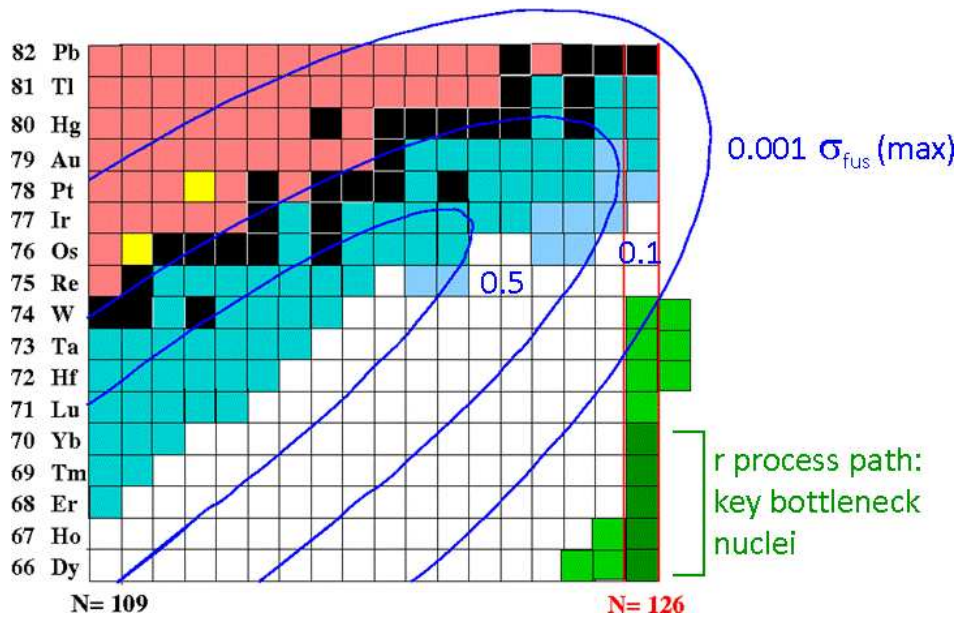


**Fig. 5** Chart of nuclides around the  $N=126$  waiting point of the  $r$ -process path. The blue ellipses denote the expected range of isotopes accessible via the novel fission-fusion process. The indicated lines represent 0.5, 0.1 and 0.001 of the maximum fusion cross section after neutron evaporation. In green the  $N=126$  nuclides relevant for the  $r$  process are marked, with the dark green colour indicating the key bottleneck nuclei for the astrophysical  $r$  process.

of the fusion yield from about  $5 \cdot 10^2$  fusion products per laser pulse to a value of up to several  $10^6$  exotic nuclides per pulse. Most likely only part of this estimated yield enhancement could finally be realized, so it may be adequate to finally quote the average between the two extremes, resulting in an estimate of about  $10^4$  fusion products generated per laser pulse. However it is obvious that collective effects from the ultra-dense ion bunches would significantly improve the experimental conditions towards the production of extremely neutron rich fusion products.

The following table finally gives a quantitative overview of the two discussed experimental scenarios with and without collective stopping reduction, based on the parameters of the 20 PW APOLLON driver laser introduced earlier. All numbers refer to yields expected for one laser pulse.

	normal stopping	reduced stopping
Th production target	$3.6 \mu\text{m}$	$3.6 \mu\text{m}$
$\text{CH}_2$ backing	$24 \mu\text{m}$	$24 \mu\text{m}$
accelerated Th ions	$10^{12}$	$10^{12}$
accelerated protons	$2 \cdot 10^{13}$	$2 \cdot 10^{13}$
accelerated C ions	$1 \cdot 10^{13}$	$1 \cdot 10^{13}$
$\text{CH}_2$ reaction target	$70 \mu\text{m}$	–
Th reaction target	$50 \mu\text{m}$	5 mm
beam-like light fragments	$2.9 \cdot 10^9$	$10^{12}$
target fission probability	$10^{-3}$	0.1
fusion probability	$1.8 \cdot 10^{-4}$	$1.8 \cdot 10^{-4}$
fusion products	$5 \cdot 10^2$	$3 \cdot 10^6$

While it will remain a challenge to directly study the key waiting point isotopes on the  $r$  process path, it is on the other hand intriguing that a wide range of so far unknown isotopes will become accessible for experimental investigation.

Presently the high-intensity APOLLON (10 PW, 150 J) laser envisaged to be used for laser ion acceleration is designed to operate at a repetition rate of one laser pulse per minute. However, laser technology is progressing rapidly with large efforts presently devoted to the development of higher repetition rates aiming of up to 1 kHz together with an increase of the laser pulse energy beyond 1 kJ. Moreover, since the yield of very neutron-rich fusion products grows strongly nonlinearly with laser energy, a final use of several coincident APOLLON laser beams would be very advantageous.

Therefore it is foreseeable that the above given estimate for the achievable rate of neutron rich fusion products can be increased within the next years significantly by several orders of magnitude.

#### 4 Experimental aspects

Exploring this 'terra incognita' of yet unknown isotopes towards the  $r$  process waiting point at  $N=126$  certainly calls for a staged experimental approach. First studies should focus on the range and electronic stopping powers of dense laser-accelerated ion beams as discussed previously, followed by systematic optimizations of target properties in order to optimize the yield of fission fragments. Subsequently the  $A$ ,  $Z$  and  $N$  distributions of the

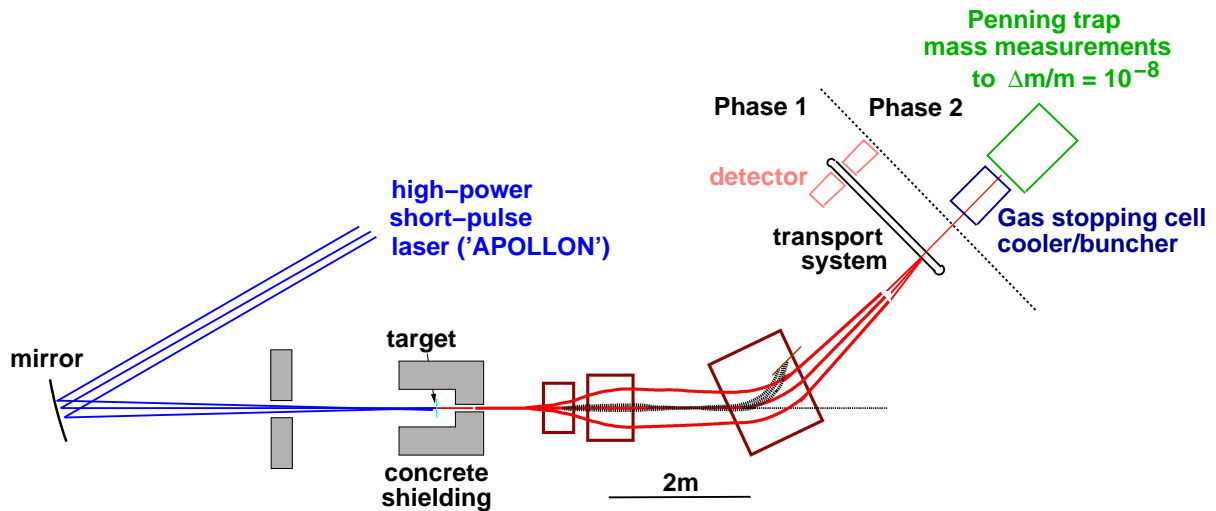


**Fig. 6** Schematical view of the experimental arrangement for fission-fusion studies. Measurements of fusion products will be performed in two stages, first aiming at an identification of the produced isotopes via decay spectroscopy using a transport system (e.g. tape), while later on precision mass measurements using a Penning trap system are envisaged.

light thorium fission fragments should be characterized. Moreover, it is unclear in how far the first neutron transfer preceding fission will additionally broaden all these distributions. Also the yields for the fusion products should be measured in exploratory experiments, where it will be crucial to optimize the kinetic energy of the beam-like fission products.

Fig. 6 shows a schematical view of the potential experimental setup of the presented reaction scenario. The high-intensity laser beam is tightly focussed onto the target assembly. This area will require heavy concrete shielding for radioprotection. The probably most essential and also most demanding experimental task will be the separation of the reaction products. Fusion products with about 2-3 MeV/u will have to be separated from faster beam-like fission fragments with about 7 MeV/u, or target-like fragments with about 1 MeV/u, which could be achieved with a velocity filter. However, the reaction products from various fusion channels varying in mass but not in velocity require a different separation scheme. Here one could use a recoil separator (as indicated in Fig. 6), where it may be advantageous to operate the separator in gas-filled mode. Alternatively also a coarse magnetic dipole pre-separator followed by a gas stopping cell and an RFQ cooler/buncher could be used to inject the ions into an electrostatic mass separator like the 'Multi-Reflection Time-of-Flight' mass spectrometer [54], especially when aiming for fusion products with lifetimes significantly shorter than 100 ms. Such a spectrometer could be operated either as isobar separator or directly for mass measurements with a mass accuracy of up to  $10^{-7}$ .

In these first studies a tape station could be used to transport the reaction products to a remote, well-shielded detector system, where the characterization of the implanted fusion products could be performed either

via  $\beta$ -decay studies (using e.g.  $\text{LaBr}_3$  scintillation detectors or  $\gamma$  spectroscopy with high-resolution germanium detectors). This scenario has been labelled in Fig. 6 with 'Phase 1'. Since most of the fusion products have typical lifetimes of  $\approx 100$  ms, they will survive the transport to a secondary target station.

In a later stage ('Phase 2'), the fusion products may be stopped in a buffer gas stopping cell [55], cooled and bunched in e.g. a radiofrequency quadrupole ion guide before then being transferred to a Penning trap system for high-accuracy mass measurements. Such a setup would be similar to the SHIPTRAP facility at GSI [56] or ISOLTRAP at ISOLDE/CERN [57] for mass measurement with an accuracy of  $m/\Delta m \sim 10^{-8}$ , corresponding to about  $10 \text{ keV}/c^2$  [58].

## 5 Conclusion

The exploration of nuclei far away from the valley of stability is a long-term endeavour of nuclear physics with strong relevance for astrophysical applications. In our present experimental proposal of a new nuclear reaction scheme we address the heavy nuclei of the  $r$ -process nucleosynthesis path towards the waiting point at  $N=126$ , where our new production scheme holds promise to bring these extremely neutron-rich isotopes into reach of direct experimental studies with significantly higher yields than accessible with classical radioactive ion beam accelerator technology. With much more compact high-power, short-pulse laser systems we intend to develop an optimized production scheme for extremely neutron-rich fusion products following induced fission from laser-accelerated ion beams. Exploiting the 'Radiation Pressure Acceleration' mechanism will allow to generate ion beams of fissile species with solid-state density. A two-

step production scheme of neutron rich nuclides ('fission-fusion') is proposed, where asymmetric fission preceded by a deep inelastic transfer reaction will be followed by fusion of the light fission fragments. Moreover, collective effects reducing the electronic stopping power in the target are expected for such ultra-dense ion bunches, allowing to use much thicker targets and thus increasing the fission yield significantly. The fusion of short-lived, neutron-rich fission fragment beams with short-lived, neutron-rich fission fragments in the target will result in very attractive production rates of extremely neutron-rich nuclides towards  $N=126$  and  $Z>70$ . Order-of-magnitude estimates promise fusion rates of about  $10^6$  fusion products per laser pulse, based on the laser parameters envisaged for the ELI-Nuclear Physics project in Bucharest (300 J, 15 fs, 20 PW). Whereas the present repetition rate of 1 laser pulse per minute limits the achievable fusion yield, ongoing development efforts for significantly higher repetition rates (aiming at up to 1 kHz) and increased laser energy (aiming at beyond 1 kJ) will open the perspective to increase the achievable yields within the fission-fusion reaction scheme by several orders of magnitude within the next years. In this way high power lasers used for laser ion acceleration can significantly contribute to access terra incognita in nuclear physics and astrophysical nucleosynthesis of heavy elements.

### Acknowledgement

We acknowledge helpful discussions with M. Heil, K.L. Kratz, H.Th. Janka and P. Ring. The authors enjoyed the collaboration with V. Zamfir, who is heading the ELI-NP project, opening up many of the new perspectives presented here. We were supported by the DFG Clusters of Excellence: 'Munich Centre for Advanced Photonics' (MAP) and 'Origin and Structure of the Universe' (UNIVERSE) and by the DFG Transregio TR18.

### References

1. K.L. Kratz et al., Prog. in Part. and Nucl. Phys. **59**, 147 (2007).
2. M. Arnould, S. Griely, K. Takahashi, Phys. Rep. **450**, 97 (2007).
3. I.V. Panov and H.-Th. Janka, Astr. Astroph. **494**, 829 (2009).
4. A. Henig et al., Phys. Rev. Lett. **103**, 245003 (2009).
5. T. Tajima, D. Habs, X. Yan, *Laser Acceleration of Ions for Radiation Therapy*, RAST, **2**, 221 (2009).
6. <http://www.eli-np.ro>
7. E. Haseltine, <http://discovermagazine.com/2002febcover>
8. C.E. Rolfs, *Cauldrons in the Cosmos*, Univ. of Chicago Press (1991).
9. K.-L. Kratz et al., Ap.J. **662**, 39 (2007).
10. H.-Th. Janka et al., Phys. Rep. **442**, 38 (2007).
11. J. Cowan and F.-K. Thielemann, Physics Today Oct., 47, 2004.
12. C. Freiburghaus et al., Ap. Jour. **525**, L121 (1999).
13. R. Surman et al., Ap. Jour. **679**, L117 (2008).
14. K. Farouqi et al., Nucl. Phys. **A758**, 631c (2005).
15. J.M. Pearson et al., Phys. Lett. **B387**, 455 (1996).
16. J.J. Cowan and C. Sneden, Nature **440**, 1151 (2006).
17. J. Dobaczewski et al., Nucl. Phys. **A 422**, 103 (1984).
18. FAIR , *An International Accelerator Facility for Beams of Ions and Antiprotons*, Baseline Technical Report, GSI (2006), <http://www.gsi.defairreportsbtr.html>.
19. SPIRAL II, *Detailed Design Study - APD Report*, GANIL (2005), <http://pro.ganil-spiral2.euspiral2what-is-spiral2apd>
20. <http://www.frib.msu.edu/aboutmsu-frib-proposal>
21. S. Baruah et al., Phys. Rev. Lett. **101**, 262501 (2008).
22. M. Dworschak et al., Phys Rev. Lett. **100**, 072501 (2008).
23. I. Dillmann et al., Phys. Rev. Lett **91**, 162031 (2003).
24. K. Blaum, Phys. Rep. **425**, 1 (2006).
25. G. Audi, A.H. Wapstra, Nucl. Phys. **A 595**, 409 (1995).
26. I.V. Panov et al., Nucl. Phys. **A747** (2005) 633.
27. P. Ring , private communication (2010).
28. P. Möller et al., Atomic Data Nucl. Data Tabl. **59**, 185 (1995).
29. B. M. Hegelich *et al.*, Nature **339**, 441 (2006).
30. H. Schwörer *et al.*, Nature **439**, 445 (2006).
31. S. Ter-Avetisyan *et al.*, Phys. Rev. Lett. **96**, 145006 (2006).
32. R. A. Snavely *et al.*, Phys. Rev. Lett. **85**, 2945 (2000).
33. E. Clarke, *et al.*, Phys. Rev. Lett. **84**, 670 (2000).
34. Maksimchuck *et al.*, Phys. Rev. Lett. **84**, 4108 (2000).
35. S. P. Hatchett *et al.*, Phys. Plasma **7**, 2076 (2000).
36. L. Robson *et al.*, Nature Physics **3**, 58 (2007) and refs. therein.
37. O. Klimo et al., Phys. Rev. ST Accl. Beams **11**, 031301 (2008).
38. A.P.L. Robinson et al., New J. Phys. **10**, 0130021 (2008).
39. S.G. Rykovanov et al., New J. Phys. **10**, 131005 (2008).
40. S. Steinke *et al.*, "Efficient ion acceleration by collective laser-driven electron dynamics with ultra-thin foils", submitted to Phys. Rev. Lett. (2009), arXiv:0909.2334v1 [physics.plasm-ph]
41. G. Mourou, The APOLLON/ILE 10 PW laser project, [http://www.nipne.ro/eli\\_np\\_workshop/contributions.php](http://www.nipne.ro/eli_np_workshop/contributions.php)
42. S. Segré, *Nuclei and Particles*, second ed., W.A. Benjamin, RA, London (1977)
43. S. Ichimaru, *Basic Principles of Plasma Physics: A Statistical Approach*, Benjamin, Reading, Ma (1973).
44. H.-C. Wu *et al.*, "Collective Deceleration"; arXiv:0909.1530v1 [physics.plasm-ph]
45. P.G. Thirolf and D. Habs, Prog. in Part. and Nucl. Phys. **49**, 325 (2002).
46. V. Metag., Nukleonika **20**, 789 (1975).
47. R. Vandenbosch and J.R. Huizenga, *Nuclear fission*, Academic Press, New York (1973)
48. Rutherford Online - Lexikon der Elemente (2006): <http://www.uniterra.derutherford>
49. A. Gavron, Phys. Rev. C **21** (1980) 230; O.B. Tarasov and D. Bazin, Nucl. Instr. Meth. **B204** (2003) 174.
50. A.B. Quint et al., Z. Phys. **A 346**, 119 (1993).
51. W. Morawek et al., Z. Phys. **A 341**, 75 (1991).

52. NRC Rare Isotope Science Assessment Committee (RISAC) Report, 2007, National Academies Press, Washington/DC, USA.
53. T. Kurtukian-Nieto, J. Benlliure, K.H. Schmidt, Nucl. Instr. Meth. A589 (2008) 472
54. W.R. Plass et al., Nucl. Instr. Meth. B266 (2008) 4560.
55. J.B. Neumayr et al., Nucl. Instr. Meth. **B244**, 489 (2006).  
J.B. Neumayr et al., Rev. Sci. Instr. **77**, 065109 (2006).
56. M. Block et al., Eur. Phys. Jour. A25 (suppl. 1) (2005) 49.
57. M. Mukherjee et al., Eur. Phys. J. A 35, 1-29 (2008).
58. M. Block et al., Nature **463**, 785 (2010).